

# Time Series and Mel-frequency Cepstrum Coefficient Analyses of Venous Pulsatile Tinnitus Vascular Sound and Flow Velocity Sensed by Transcranial/Retroauricular Doppler Ultrasound Approaches

Yue-Lin Hsieh,<sup>1,2</sup> Yue-Da Hsieh,<sup>3</sup> and Wuqing Wang<sup>1,2\*</sup>

<sup>1</sup>Department of Otolaryngology and Skull Base Surgery, Eye, Ear, Nose, & Throat Hospital, Fudan University, No. 83 Fenyang Rd., Xuhui Dist., Shanghai 200031, China

<sup>2</sup>NHC Key Laboratory of Hearing Medicine, No. 83 Fenyang Rd., Xuhui Dist., Shanghai 200031, China

<sup>3</sup>Department of Economics, London School of Economics and Political Science, London WC2A 2AE, United Kingdom

(Received March 29, 2022; accepted May 16, 2022; online published June 23, 2022)

**Keywords:** pulsatile tinnitus, correlation analysis, transcranial Doppler ultrasound, time series, Mel-frequency

Venous pulsatile tinnitus (PT) arises from the motion of blood flow. However, the correlation between flow velocity and amplitude remains undiscovered. In this study, retroauricular color-coded Doppler (RCCD) and transcranial color-coded Doppler (TCCD) ultrasound examination techniques were deployed to assess the hemoacoustics at the ipsilateral internal jugular vein (IJV), intradiverticular, mainstream sinus, and transverse sinus regions. Auto- and cross-correlation analyses were used to analyze the correlations between flow velocity and amplitude. Furthermore, the Mel-frequency cepstrum coefficients were calculated, and the Mel-spectrogram was used to exhibit the human perception of PT. The mainstream sinus flow had the highest coefficient (cross-correlation coefficient = 0.781) among the sensed locations. The cross-correlation coefficient of the IJV was the second largest and close to that of the mainstream sinus flow. The transverse sinus flow had the lowest cross-correlation coefficient. Additionally, the transverse sinus septum was visualized for the first time using the RCCD technique in this study. In conclusion, cross-correlation analysis indicates that the amplitude of vascular sound is highly correlated to the vascular flow velocity. The Mel-spectrogram demonstrates the outcome of the human perception of PT, and its use can be extended to future psychoacoustic studies.

## 1. Introduction

Vascular pulsatile tinnitus (PT) is categorized by the abnormal perception of the dural venous sinus blood flow somatosound.<sup>(1)</sup> This type of tinnitus is subcategorized under objective tinnitus, for which anatomical lesions or vascular sound can be objectively found or perceived by an observer.<sup>(2)</sup> Venous PT is the most common vascular PT,<sup>(3)</sup> which can be silenced or reduced by

---

\*Corresponding author: e-mail: [wuqing@eent.shmu.edu.cn](mailto:wuqing@eent.shmu.edu.cn)  
<https://doi.org/10.18494/SAM3917>

digital compression over the ipsilateral internal jugular vein (IJV). Despite various causative and contributory factors of PT, the most common abnormal anatomical findings are sigmoid sinus wall anomalies (SSWAs), namely, sigmoid sinus wall dehiscence and sigmoid sinus diverticula.<sup>(4)</sup>

The perturbation of blood flow and increased central venous pressure near SSWAs have been suggested to augment the acoustic amplitude of PT.<sup>(5,6)</sup> Vibroacoustic and hydroacoustic generation of sound are two major acoustic sources of venous PT associated with SSWAs.<sup>(7,8)</sup> As the sigmoid plate becomes dehiscent, the sound of sigmoid sinus vascular wall displacement (vibroacoustic source) secondary to flow impingement and blood flow motion (hydroacoustic source) is transmitted to the inner ear via the air-conduction transmission route.<sup>(9)</sup> Although the clinical association among SSWAs, transverse sinus stenosis, and idiopathic intracranial hypertension has been increasingly investigated and identified by clinicians,<sup>(4)</sup> no conclusion has been drawn on the correlation between hemodynamics and the acoustic production of PT.

Vascular Doppler ultrasound works by measuring sound waves that are reflected from moving objects such as red blood cells.<sup>(10)</sup> The frequency shift, which is exhibited as a spectrum, is determined by all the factors associated with the Doppler equation. Higher velocities produce shifts to higher frequencies.<sup>(11)</sup> Doppler ultrasound examination of venous flow can be used to capture the *in vivo* hydroacoustic source of PT.<sup>(7,12)</sup> Since the depth and width of flow sampling are adjustable, different directions and locations of blood flow can be detected.<sup>(10)</sup> In previous studies, the vascular sound sampled at the upper IJV exhibited high accordance with participants' subjective perception of PT in terms of rhythm and frequency.<sup>(12)</sup> Nevertheless, the transverse-sigmoid junction is the most common location of SSWAs. Since Doppler ultrasound simultaneously reflects hemodynamics and acoustics, insonation at the transverse-sigmoid junction can be used to directly obtain the focal hydroacoustic characteristics of blood flow.

While pulse-synchronous vascular sound is the main chief complaint of patients with venous PT, the correlation between the flow velocity and amplitude of venous PT, however, has remained little recognized. This study aims to reveal the bioinformatics of venous PT by using retroauricular color-coded Doppler (RCCD) and transcranial color-coded Doppler (TCCD) approaches.

## 2. Materials and Methods

### 2.1 Study design

A 46-year-old female patient with right-sided venous PT was examined in this study. The duration of her PT was 7 months, and PT was eliminated when the ipsilateral IJV was compressed. Contrast-enhanced computed tomography (CT) evidenced a large protrusive sigmoid sinus diverticulum on her right ear. The diagnosis of venous PT strictly followed our previously established clinical protocols.<sup>(9)</sup>

This study was designed using mathematical methods to analyze the vascular flow and acoustic display sensed by a LISENDO 880 ultrasound system (Hitachi Aloka Medical Ltd., Japan) with S121/L441 transducers. Additionally, 1) the acoustic sound was recorded using a microphone (VideoMicro, RODE, Sydney, Australia) oriented to the speakers of the ultrasound

system, 2) the electrocardiogram was installed on the participant, and 3) to synchronize image and acoustic data, a camera was placed on a support facing the Doppler monitor. The Doppler velocity spectra, acoustic profile, and subjective/objective audio perception of venous PT were the major goals of this study. The locations of Doppler insonation were the a) transverse sinus, b) intradiverticular flow, c) transverse-sigmoid sinus mainstream, and d) IJV. A complete setup of the sensing platform is displayed in Fig. 1.

The participant in this study provided written informed consent. Experimental measurements were conducted in accordance with the Declaration of Helsinki. Ethics approval was obtained from the Ethical Committees of the Eye, Ear, Nose, & Throat Hospital in Shanghai, China.

## 2.2 RCCD and TCCD sensing techniques

The RCCD technique was implemented to assess mainstream and intradiverticular flows. The participant's CT images were carefully studied prior to Doppler insonation to accurately localize the transverse-sigmoid sinus mainstream and intradiverticular flows. B-mode and color mapping were alternately used to visualize the anatomical and flow structures (Fig. 2). In addition to diverticular structures, a laterally placed sigmoid sinus and intravascular structures such as a transverse sinus septum can be visualized (Fig. 3). Detailed descriptions of the RCCD and TCCD techniques have recently been reported by our research group.<sup>(13)</sup>

In brief, to reveal the mainstream and intradiverticular hydroacoustic characteristics, coronal and sagittal footages of the diverticulum and blood flow were visualized under the B-mode and/or color mode using a linear L441 transducer (see Fig. 2 for anatomical features). As shown in Fig. 2, a thin layer of mastoid bone is present at the medial surface of the diverticulum. This typical remanent bone structure isolates diverticular and mainstream flows and serves as a referencing landmark. Therefore, we analyzed both intradiverticular and mainstream sinus

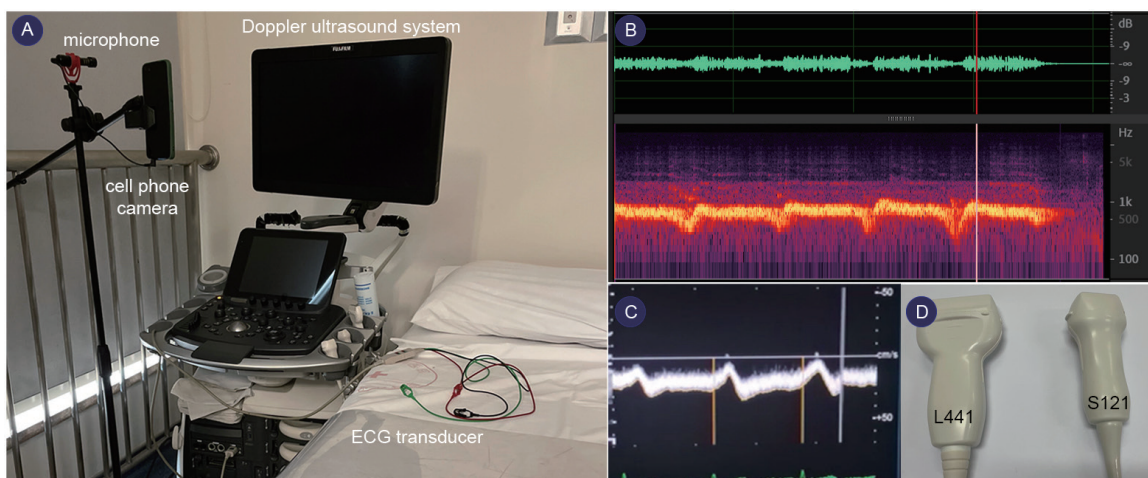


Fig. 1. (Color online) (A) Complete setup of the sensing platform. (B) and (C) Synchronization of audio profile and Doppler flow velocity. (D) Doppler linear L441 transducer (12 to 2 MHz) and sector S121 transducer (5 to 1 MHz).

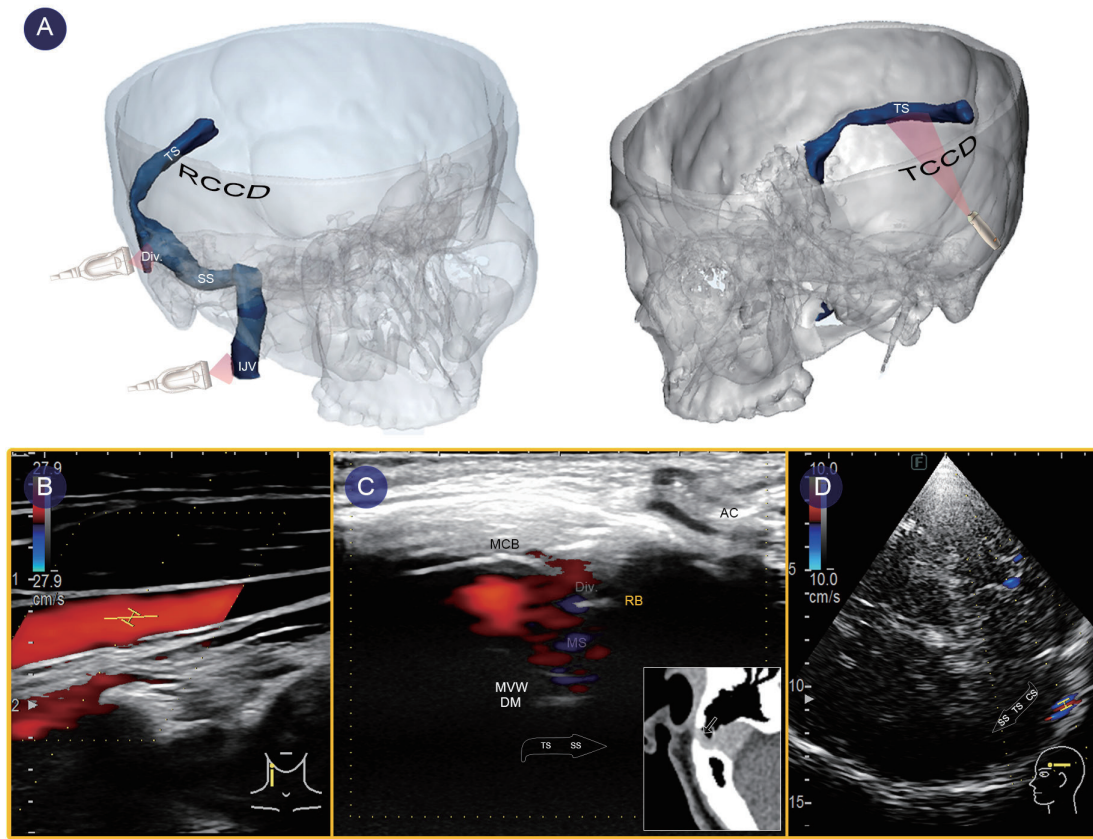


Fig. 2. (Color online) (A) Schematic diagram of RCCD, TCCD, and cervical Doppler examination. (B) Measurement of IJV. (C) Measurement of intradiverticular and mainstream sinus flows using RCCD method. (D) Measurement of transverse sinus flow using TCCD method. MCB: mastoid cortical bone; Div.: diverticulum; MS: mainstream; RB: remnant mastoid bone; MVW and DM: medial vascular wall and dura mater, respectively; CS: confluens sinuum; SS: sigmoid sinus; and TS: transverse sinus. The white arrow indicates the flow direction.

flows in this study using the RCCD method. The sampling width was set at 1 to 3 mm based on the width of the detected vessel as appropriate. The depth was adjusted between 3 to 4.5 cm on the basis of intrasubject variability. The transducer frequency was 4.0 to 5.22 MHz. The color Doppler gain was then adjusted from 20 to 120.<sup>(13)</sup>

For the TCCD method, the detection of the transverse sinus flow was performed using an S121 probe insonated from the contralateral temporal bone window. A low wall filter and low-flow sensitive settings were adopted. The great cerebral vein was found, and the rostral part of the superior sagittal sinus was visualized successively. The torcular herophili was discovered by tracking along the course of the straight sinus, which drains posteriorly into the occipital region. The contralateral transverse sinus was found subsequently. The depth was adjusted between 10 and 15 cm according to individual differences. The sample volume was set at 1 to 3 mm as appropriate on the basis of the width of the detected vessel. The transducer frequency ranged from 1.5 to 1.88 MHz, and the color gain was adjusted between 20 and 120.<sup>(13)</sup>

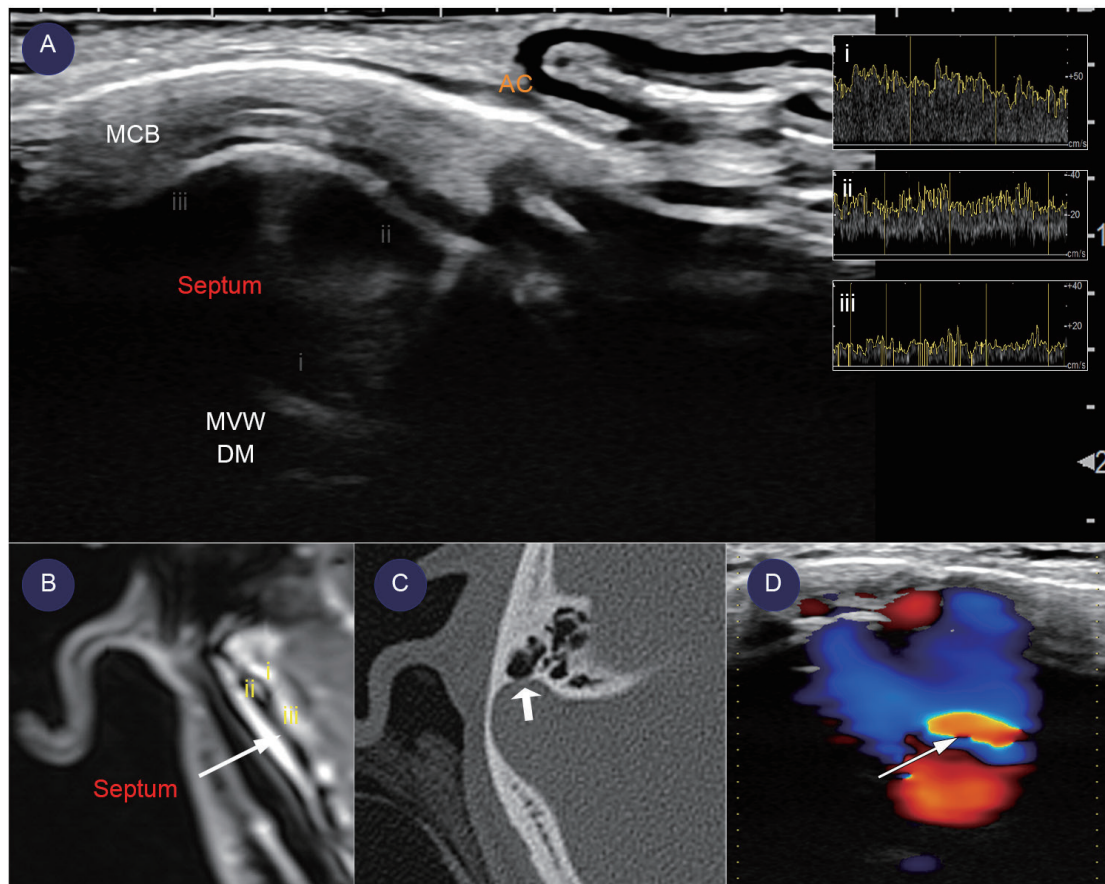


Fig. 3. (Color online) Exceptional case illustrating flow characteristics in PT patient with transverse sinus septum and laterally placed sigmoid sinus encountered in our PT clinic. (A) B-mode visualization of transverse sinus septum using RCCD technique. i: mainstream sinus flow; ii: flow measured at circular shape of transverse sinus septum; and iii: flow measured posterior to circular shape of transverse sinus septum. (B) Image of transverse sinus septum using axial T1-3D volumetric interpolated breath-hold (VIBE) magnetic resonance venogram sequence. (C) CT image of patient demonstrating lateral placed sigmoid sinus with sigmoid plate dehiscence. (D) Visualization of septal flow (white arrow) using the continuous wave mode via RCCD method. AC: auricular cartilage; MCB: mastoid cortical bone; and MVW and DM: medial vascular wall and dura mater, respectively.

### 2.3 Data extraction and preprocessing

The velocity spectra of four specific anatomical locations were obtained using an image recognition method scripted by MATLAB R2017a (MathWorks). To unify the time units of velocity and amplitude spectra, we trimmed the total time length of the spectra to 2.149 s with 0.001 s per time unit using an interpolation method. Prior to data analysis, the flow acoustics were aligned using Adobe Audition 2020 software (Adobe Inc., United States). For the acoustic analysis of the flow sound, positive values of the spectrotemporal results of the acoustic data were enveloped (Fig. 4).

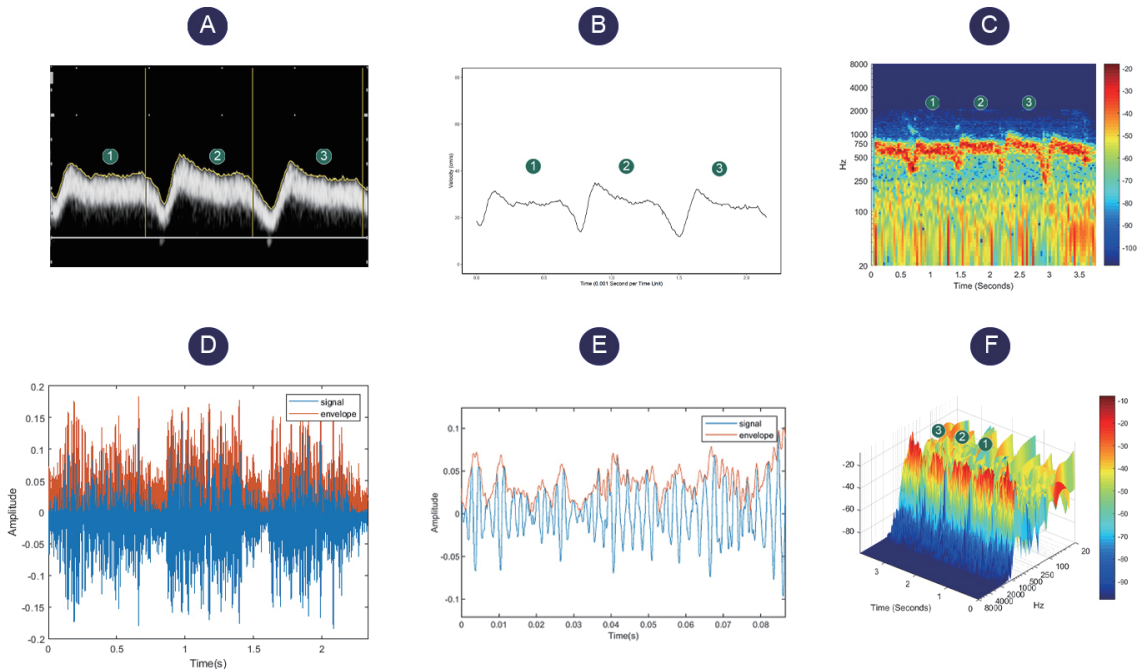


Fig. 4. (Color online) Demonstration of signal processing of measured IJV hemoacoustics of participant. (A) Inverted IJV Doppler flow spectra. (B) Acquired IJV Doppler flow spectra. (C) Spectrotemporal diagram of IJV flow calculated using short-time Fourier transform. (D) Complete view envelope of acquired IJV flow amplitude. (E) Enlarged view of acquired IJV flow amplitude at time frame within 0.01 s. (F) Three-dimensional waterfall diagram of IJV flow calculated using short-time Fourier transform.

## 2.4 Autocorrelation analysis of Doppler velocity spectra

To examine the randomness of the time and frequency domains of all series, the Ljung–Box test was calculated using R software version 3.4.3 (RStudio, United States):

$$Q(m) = T(T+2) \sum_{i=1}^m \frac{\hat{p}_i}{T-i}, \quad (1)$$

where  $T$  is the sample quantity,  $m$  is a manually selected number, and  $\hat{p}_i$  is the correlation coefficient of the number of lag  $i$ .

The augmented Dickey–Fuller test was applied to test the stationarity of the series, which can be presented as

$$\Delta Y_t = \alpha + \beta_t + \delta Y_{t-1} + \sum \lambda_i \Delta Y_{t-i} + e_i, \quad (2)$$

where  $\Delta Y$  is the first difference of  $Y$ .  $\alpha$  and  $\beta$  are included to establish the existence of a deterministic trend, indicating possible data stationarity. The unit root test was carried out under the null hypothesis  $\delta = 0$ . The negativity of  $\delta$  in the above equation was tested using

$$DF_{\tau} = \frac{\hat{\delta}}{SE(\hat{\delta})}, \quad (3)$$

which was calculated to compare relevant critical value for the Dickey–Fuller test. No unit root is present if the calculated test statistic is more negative than the critical value for which the null hypothesis of  $\delta = 0$  is rejected.

The autocorrelation function (ACF) and partial ACF (PACF) were analyzed to examine the internal structure of the analyzed series. The ACF  $\rho(k)$  is the linear correlation coefficient between  $z_t$  and  $z_{t-k}$  at lag  $k$  ( $k = 0, 1, 2, \dots$ ) of the  $z_t$  series:

$$\rho_k = \frac{Cov(z_t, z_{t-k})}{\sqrt{Var(z_t)Var(z_{t-k})}}. \quad (4)$$

The PACF is the linear correlation between  $z_t$  and  $z_{t-k}$ , using which the possible effects of relationships among values at intermediate lags are controlled.

## 2.5 Cross-correlation analysis of velocity spectra and flow amplitude

Cross-correlation was used to measure the similarity of two series as a function of the lag and the lead of one series relative to the other. The correlation between flow velocity and filtered flow amplitude was examined. The cross-correlation function was evaluated using R software:

$$r = \frac{\sum_i [(X_{(i)} - mX) * (Y_{(i-d)} - mY)]}{\sqrt{\sum_i [(X_{(i)} - mX)]^2} \sqrt{\sum_i [(Y_{(i-d)} - mY)]^2}}, \quad (5)$$

where  $mX$  and  $mY$  are the mean values of the corresponding time series. If all time points are calculated, then  $d = 0, 1, 2, \dots, N - 1$  and a correlated series twice as large as the original series can be obtained. The order of lags and leads was set at  $10^6$ .

Because the amplitude of acoustic data fluctuates drastically, the Hodrick–Prescott (HP) filter was applied to smooth the acoustic signals using Eviews software (IHS Global Inc, United States) (Fig. 5):

$$\min_{\hat{\delta}} \left( \sum_{t=1}^T (y_t - \tau_t)^2 + \lambda \sum_{t=2}^{T-1} [(\tau_{t+1} - \tau_t) - (\tau_t - \tau_{t-1})]^2 \right), \quad (6)$$

where the sum of the squared deviations  $d_t \equiv y_t - \tau_t$  penalizes the cyclical component, and the second term penalizes variations in the growth rate and is a multiple  $\lambda$  of the sum of the squares of the trend component's second differences.  $\lambda$  was set at  $10^6$  for the analysis of all series.

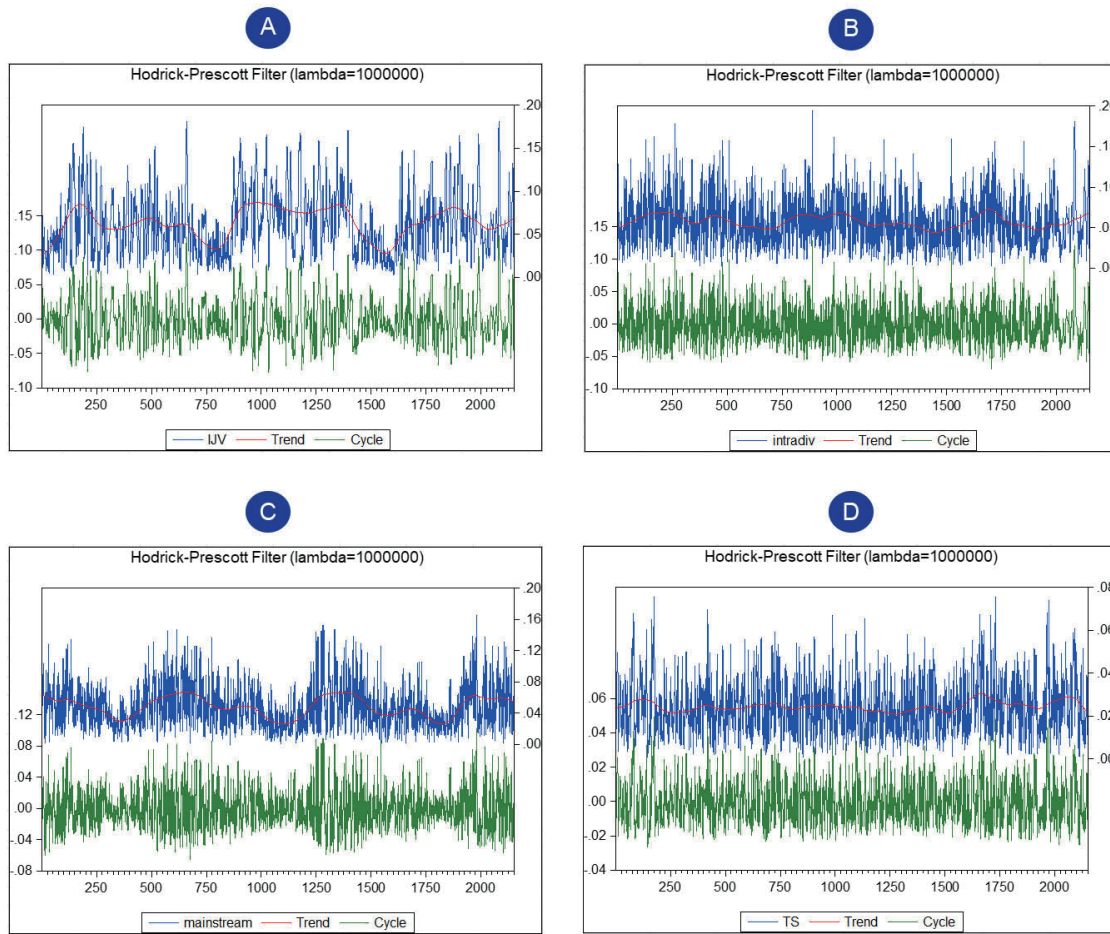


Fig. 5. (Color online) Hodrick–Prescott (HP) filter of flow amplitude measured at (A) IJV, (B) intradiverticulum, (C) mainstream sinus, and (D) transverse sinus flows.

## 2.6 Mel-frequency cepstral coefficient and Mel-spectrogram

The Mel-frequency cepstrum is a linear cosine transform of a log power spectrum on a nonlinear Mel scale of frequency that represents the short-term power spectrum of a sound. Mel-frequency cepstral coefficients (MFCCs) are the coefficients constituting the Mel-frequency cepstrum. The MFCC feature extraction technique, a non-parametric method for modeling the human auditory perception system, approximates the response of the human auditory system more closely than linearly spaced frequency bands.<sup>(14)</sup> Since MFCCs are based on the known variation of the human ear's critical bandwidth with the frequency, we calculated MFCCs to observe differences between the human perception and the objectified acoustic profile of PT using MATLAB. The MFCC extraction method consists of four major steps: 1) frame blocking and Hamming windowing, 2) fast Fourier transform, 3) triangular bandpass filters, and 4) discrete cosine transform and calculation of the log energy. A complete workflow is shown in Fig. 6. MFCCs were performed using a Hamming window of 8192 samples, and the number of coefficients was 32. The signal within a frame was assumed periodic. The Mel scale relates the

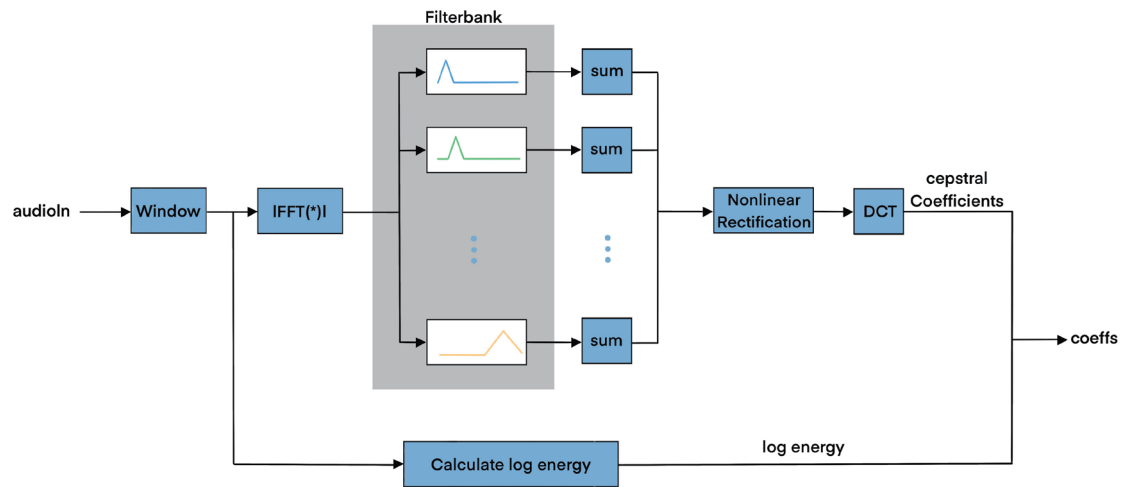


Fig. 6. (Color online) Procedure of MFCC signal processing.

perceived frequency, or pitch, of a pure tone to its actual measured frequency, which is related to the common linear frequency  $f$  by the equation

$$mel(f) = 1125 * \ln(1 + f / 700). \quad (7)$$

Triangular bandpass filters were used to smooth the magnitude spectrum and reduce the size of the features involved. For the calculation of MFCC spectrogram, samples of Hamming window were 4096, and the band number was 256. The discrete cosine transform was used to transform the frequency domain into a time-like domain called the quefrequency domain:

$$C_m = \sum_{k=1}^N \cos \left[ m * (k - 0.5) * \frac{\pi}{N} \right] * E_k, \quad m = 1, 2, \dots, L, \quad (8)$$

where  $N$  is the number of triangular bandpass filters and  $L$  is the number of Mel-scale cepstral coefficients.

To display spectrotemporal results, the short-time Fourier transform (STFT) of PT was performed in line with our previous reports using MATLAB R2017a (MathWorks):

$$STFT \{x[n]\}(m, \omega) \equiv X(\tau, \omega) = \sum_{n=-\infty}^{\infty} x[n] w[n-m] e^{-j\omega n}, \quad (9)$$

where  $x[n]$  denotes the sequence of discretized time-domain signals to be transformed,  $m$  is the time index,  $\omega$  is the frequency, and  $w[n]$  denotes the sequence of discretized window functions. The method and parameters used in the transformation method have been described. The subject was asked to rate the likeness of audio profiles using a visual analog scale (VAS) from 0 to 10.

### 3. Results

The complete hemodynamic results are shown in Table 1. The mean and peak velocity at the IJV were 22.8 and 31.0 cm/s, respectively, which were larger than those of other detected regions based on results obtained by the ultrasound system. The velocity of the mainstream sinus flow was the smallest (mean velocity: 7.2 cm/s; peak velocity 10.4 cm/s) among the detected regions, possibly because of the existence of the transverse sinus septum.

All series were non-random in this study (Ljung–Box test,  $p < 0.05$ ). The augmented Dickey–Fuller test results are shown in Table 2. The augmented Dickey–Fuller test demonstrated the existence of no unit root among the tested series ( $p < 0.01$ ), indicating that all the series were stationary. All series showed a decaying ACF with periodic characteristics (Fig. 7). This indicated that the autocorrelation decreased as the lag increased among the observed series. Although all series showed pulsating trends in the flow velocity spectrum, the PACF plot exhibited a strongly periodic correlation in the IJV series with more consistent equal-spaced timepoints than at other locations (Fig. 7).

The results of the cross-correlation between flow velocity and amplitude are shown in Fig. 8 and Table 3. The mainstream sinus flow had the highest coefficient among the tested series, and the participant considered the mainstream sinus flow sound to most closely resemble her PT (Supplementary File 1). The coefficient of the IJV was second largest and close to that of the mainstream sinus flow. The transverse sinus flow had the lowest coefficient.

The results of the MFCCs are shown in Fig. 9. The frequency of PT predominantly fluctuated between 0 Hz and 3 kHz, wherein the amplitude in the low-frequency range (below 100 Hz) of PT was less impactful on human subjective perception than those calculated using the STFT. The major power of the frequency predominantly fluctuated below 1 kHz. Note that pulsatory fluctuation of the frequency range above 1 kHz was observed in all locations. An audio file of the retrieved MFCC data of the mainstream sinus (audio data that was selected as most

Table 1  
Doppler hemodynamic results of IJV, intradiverticular, mainstream sinus, and transverse sinus flows.

	Unit	IJV	Intradiverticular	Mainstream	TS
Peak velocity	cm/s	31.0	11.9	10.4	20.6
Mean velocity	cm/s	22.8	7.7	7.2	17.1
Resistive index		0.340	0.468	0.426	0.459
Pulsatility index		0.462	0.723	0.616	0.553

IJV: internal jugular vein; TS: transverse sinus.

Resistive and pulsatility indices are dimensionless.

Table 2  
Augmented Dickey–Fuller results of IJV, intradiverticular, mainstream sinus, and transverse sinus flows.

	IJV	Intradiverticular	Mainstream	TS
Augmented Dickey–Fuller	−5.463	−3.606	−3.512	−5.979
Lag length	24	25	19	9
$p$ -value	<0.01	<0.01	<0.01	<0.01

IJV: internal jugular vein; TS: transverse sinus.

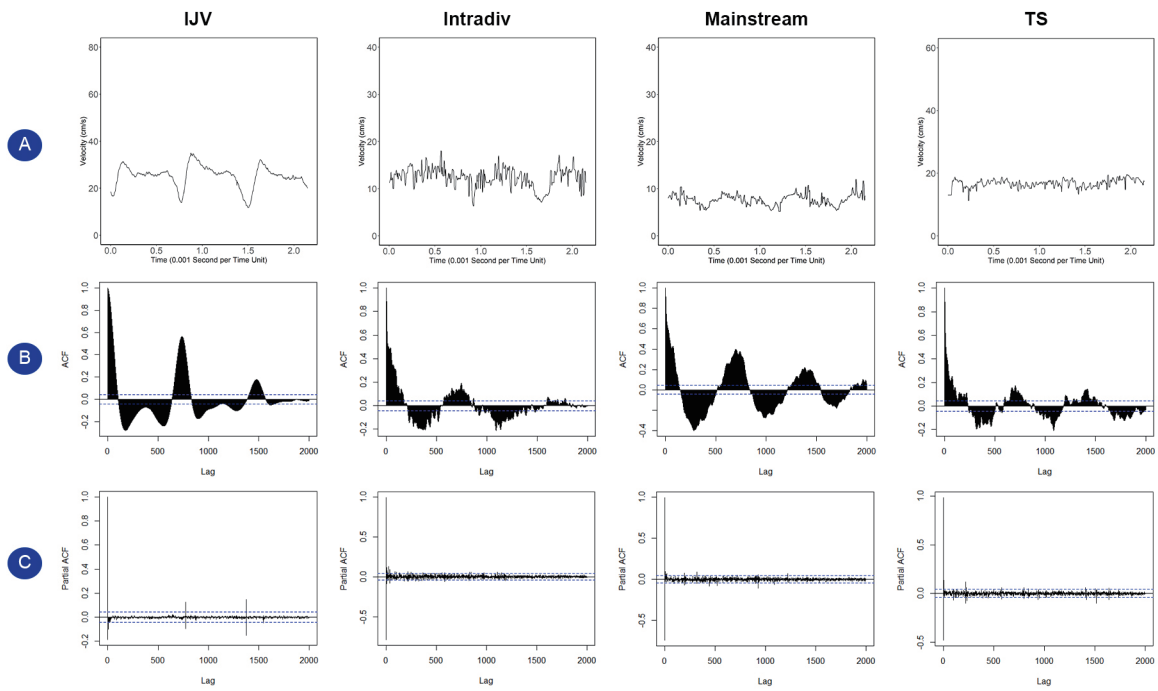


Fig. 7. (Color online) (A) Doppler flow velocity spectrum of IJV, intradiverticular, mainstream sinus, and transverse sinus flows. (B) Results of ACF for all tested flow velocity spectra. (C) Results of PACF for all tested flow velocity spectra.

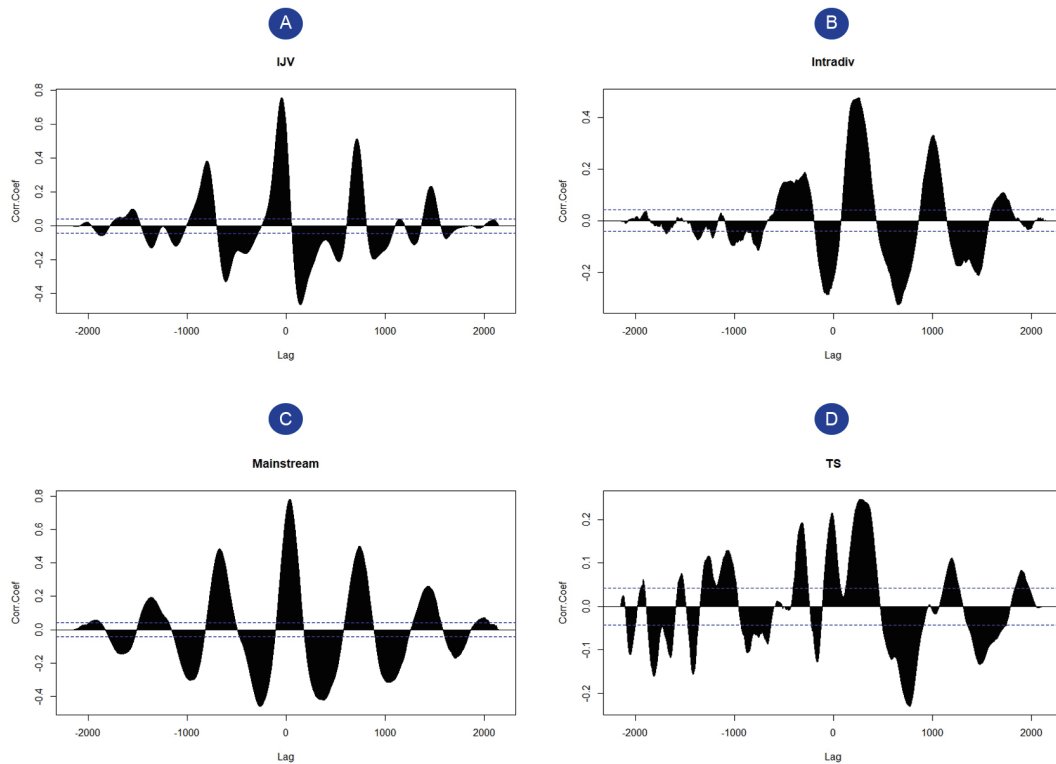


Fig. 8. (Color online) Results of cross-correlation analysis of flow velocity and flow amplitude. Corr.Coeff indicates the correlation coefficient. Correlation coefficients of (A) IJV, (B) intradiverticular, (C) mainstream sinus, and (D) transverse sinus flows.

Table 3

Cross-correlation coefficients of IJV, intradiverticular, mainstream sinus, and transverse sinus flows.

	IJV	Intradiverticular	Mainstream	TS
Coefficient	0.75822	0.47691	0.78110	0.247207
Lag	2106	2409	2189	2421

IJV: internal jugular vein; TS: transverse sinus.

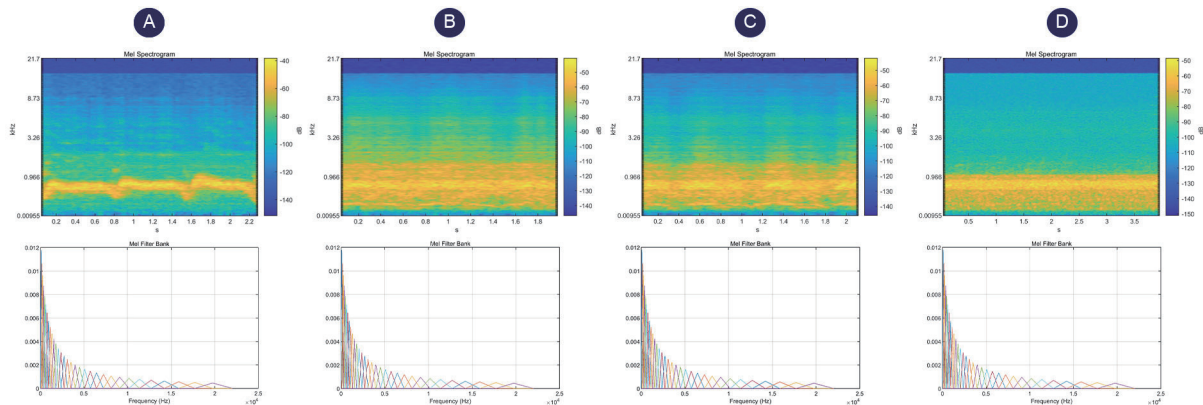


Fig. 9. (Color online) Mel spectrograms of PT measured at different anatomical locations. (A) Upper IJV, (B) intradiverticulum, (C) transverse-sigmoid junction mainstream, and (D) transverse sinus.

resembling the participant's PT) was output (Supplementary File 2). The likeness of the MFCCs audio profile rated by the participant (score = 9) was higher than that of the original acoustic profile (score = 8).

## 4. Discussion

### 4.1 Correlation between flow amplitude and flow velocity based on Doppler sensing

Given the current correlation results, the Doppler ultrasound revealed a close relationship between the sampled flow velocity and flow amplitude of the hydroacoustic source, where the mainstream sinus and IJV flows showed higher coefficients than the intradiverticular and transverse sinus flows. Two factors may potentially lead to this disparity. First, the intradiverticular flow consists of multidirectional vortices, as indicated by the loss of the spectral window and the broadening of the spectrum at the transverse-sigmoid junction. The vortical flow structure may act as a pivotal influencing factor lowering the correlation coefficient. Second, the TCCD method involves a deep sensing length, for which a poor temporal window may reduce the strength and clarity of Doppler signals.<sup>(13)</sup> Nonetheless, as the mainstream sinus and intradiverticular flows are insonated at the same location, it is therefore more likely that the intradiverticular vortical flow component lowered the correlation coefficient.

The current finding substantiates the previous surgical hypothesis suggesting that the reduction of flow velocity near the hearing apparatus is pertinent to resolving PT. According to

previous computational studies, reducing the fluctuation of the flow velocity alleviates the wall pressure induced by the fluid–structure interaction and reduces the vibroacoustic component of PT.<sup>(6,15)</sup> Thus, if surgical reduction of the flow velocity is prioritized, the endoluminal stenting technique may be more suitable than the transtemporal technique since expanding the sinus lumen endoluminally is less likely to perniciously augment the intracranial pressure.<sup>(7,16,17)</sup> In contrast to transverse sinus stenting, using the transtemporal compression technique to reduce the flow velocity should prevent overcompressing the sinus lumen to avoid the iatrogenic cause of intracranial hypertension.<sup>(16)</sup> Nonetheless, the flow volume and/or flow velocity can be effectively redistributed or reduced locally after external compression, whereas local compression over the prominent transverse-sigmoid junction will not significantly impair bilateral flow dynamics *in vivo*.<sup>(9)</sup> Therefore, the degree of reduction of flow velocity and the patency of collateral sinuses should be carefully measured prior to surgical intervention. Since the surgical repair of dehiscence using robust biomaterials provides a therapeutic effect in alleviating PT,<sup>(15)</sup> the external compression technique can be performed as an additional or alternative method if addressing dehiscence alone fails to preclude PT.<sup>(10)</sup> Further studies on the range of velocity reduction and its surgical indication to eliminate PT are warranted.

#### **4.2 Sinus hemodynamics and possible presurgical curative indicator for elimination of PT**

Intracranial venous return is largely propelled by the negative pressure induced by ventricular filling while the flow velocity rises steeply and drops during ventricular ejection based on real-time ECG detection. According to our recent published data for 19 subjects investigated using the RCCD method,<sup>(13)</sup> PT disappears as the velocity drops by approximately 50% during manual compression over the ipsilateral IJV. However, in our study subject, the flow velocity at the transverse-sigmoid junction is comparatively low with a mean velocity of approximately 7 to 12 cm/s as shown in Fig. 10. This raises the question of whether addressing the transverse sinus stenosis can reduce the flow velocity or is pertinent to the endoluminal surgical goal since the sinus velocity is comparatively low prior to surgical intervention. Note, however, that the range of reduction of the flow velocity required to relieve PT varies drastically among subjects.<sup>(10)</sup> Nonetheless, the RCCD and ipsilateral IJV compression techniques may potentially provide a presurgical individual baseline curative indicator for reducing the flow velocity at the transverse-sigmoid junction in subjects with a protrusive diverticulum and laterally placed sigmoid sinus, for which further case studies are warranted.

#### **4.3 Mel-spectrogram analysis and future direction of investigation**

The main power of PT predominantly falls within low frequencies.<sup>(1,18)</sup> In this study, the Mel-spectrogram revealed similar patterns to those calculated by the STFT method. However, a prominent difference between the MFCC and STFT methods appears at frequencies below 100 Hz. Since the Mel-frequency is proportional to the logarithm of the linear frequency,<sup>(14)</sup> it exhibits a practical human auditory perception of PT. Additionally, the Mel-spectrogram

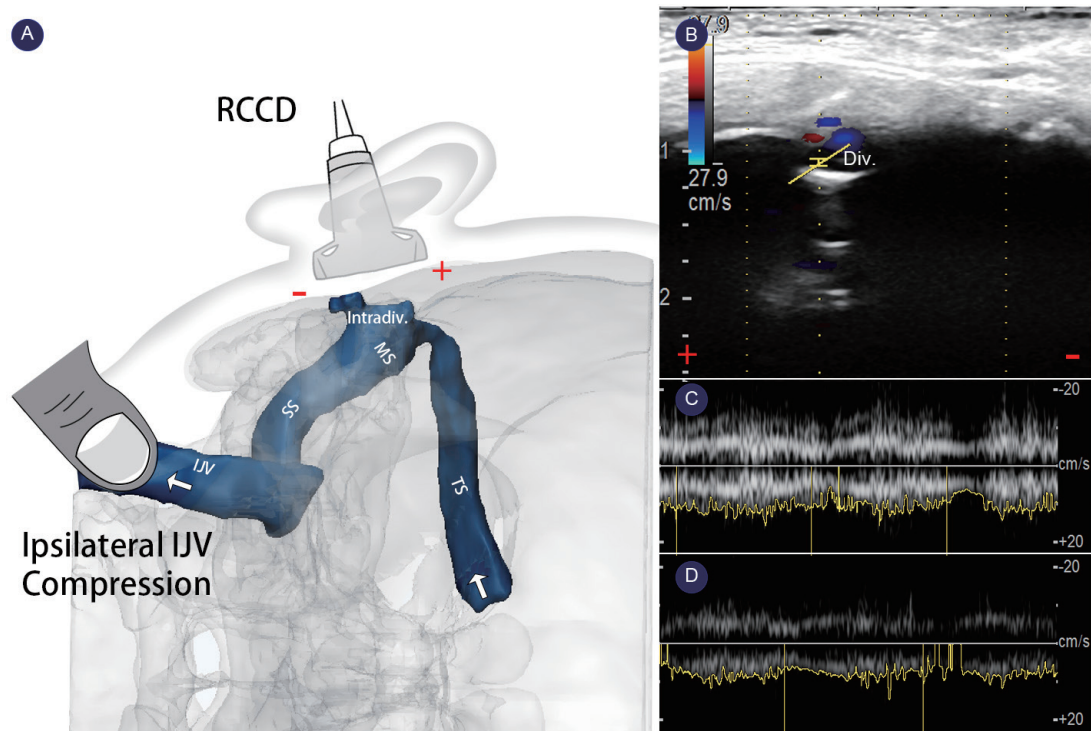


Fig. 10. (Color online) RCCD and upper ipsilateral IJV compression method as a presurgical curative indicator for elimination of PT. (A) Three-dimensional reconstruction of patient's temporal bone and schematic diagram of RCCD and ipsilateral IJV compression technique. (B) Doppler sampling of flow velocity inside diverticulum (C) before and (D) after IJV compression. +: superior direction; -: inferior direction; TS: transverse sinus; MS: mainstream sinus; Intradiv.: intradiverticulum; SS: sigmoid sinus; and IJV: internal jugular vein.

validates the fact that the high-frequency component of PT may also be perceived by some patients. This has been confirmed by some test subjects who found 1/3 octave narrow-band noise with 1 kHz center frequency resembling their PT during psychoacoustic frequency matching.<sup>(7)</sup>

#### 4.4 Transverse sinus septum and flow impact on transverse-sigmoid sinus junction

A transverse sinus septum is a common anatomical variation found in the normal population.<sup>(19)</sup> As demonstrated in Fig. 3, flow characteristics differ among different septal regions. Since the Doppler method is limited in providing a comprehensive view of the septum, it is currently unknown how septal variations impact on PT hydroacoustic characteristics. However, the septum can be a natural barrier inside the lumen that causes speed differentiation or engenders vortices due to septal structures not parallel to the flow direction. In addition to hemodynamic studies, further studies on the safety of extraluminal and endoluminal surgical methods and the influence of the transverse sinus septum on the hydroacoustic characteristics of PT are warranted.

#### 4.5 Study limitation

The main limitation of this study is the analysis of flow acoustics based on the primitive external recording system. The original data of the displayed Doppler audio was unobtainable from the medicalized/commercialized ultrasound system. Second, although this study was a case study, we focused on the correlation between Doppler and acoustic spectra, i.e., the mechanism of flows. The current Doppler mechanism based on this ultrasound system should be applicable to other cases, although further investigation is warranted. Intracranial arteriovenous malformation is not uncommon in patients with PT. Fundamental differences between flow acoustics and arterial/venous flow and cardiac phases may exist among different vascular origins of PT. This is to be discussed in our future studies.

#### 5. Conclusions

On the basis of the findings obtained from the current ultrasound system and the implementation of the Doppler method, the following are concluded:

- Cross-correlation analysis indicates that the amplitude of vascular sound is highly correlated to the vascular flow velocity.
- According to the results of real-time ECG detection, the sinus flow velocity rises steeply during ventricular filling and drops during ventricular ejection, which indicates that the sinovenous flow is predominantly propelled by the diastole of the heart instead of the upstream intracranial pressure.
- The Mel-spectrogram approximates the outcome of human perception of PT, and its use can be extended to future psychoacoustic studies.
- A transverse sinus septum may induce complex flow patterns and velocity differentiation at the transverse-sigmoid junction that can be visualized and measured by the RCCD method.
- The RCCD method is viable for acquiring in vivo hydroacoustic characteristics from patients with a protrusive diverticulum and a laterally placed sigmoid sinus, which can be applied in a junction alongside an ipsilateral IJV compression test to reveal a presurgical curative hemodynamic indicator for the elimination of PT.

#### Acknowledgments

Y.-L. Hsieh and Y.-D. Hsieh contributed equally to this work. W. Wang was supported by the National Natural Science Foundation of China (No. 81670933) and Natural Science Foundation of Shanghai (No. 20ZR1409600).

#### References

- 1 J. J. Song, G. S. An, I. Choi, D. De Ridder, S. Y. Kim, H. S. Choi, J. H. Park, B. Y. Choi, J. W. Koo, and K. Lee: *Otol. Neurotol.* **37** (2016) 613. <https://doi.org/10.1097/MAO.0000000000001005>
- 2 A. Sismanis: *Curr. Opin. Otolaryngol. Head Neck Surg.* **19** (2011) 348. <https://doi.org/10.1097/MOO.0b013e3283493fd8>

- 3 S. H. Kim, G. S. An, I. Choi, J. W. Koo, K. Lee, and J. J. Song: PLoS One **11** (2016) e0157722. <https://doi.org/10.1371/journal.pone.0157722>
- 4 D. J. Eisenman, P. Raghavan, R. Hertzano, and R. Morales: Laryngoscope **128** (2018) S1. <https://doi.org/10.1002/lary.27218>
- 5 S. Tian, X. Fan, Y. Wang, Z. Liu, and L. Wang: J. Biomech. **84** (2019) 197. <https://doi.org/10.1016/j.jbiomech.2018.12.049>
- 6 Z. Mu, Y. Sun, X. Li, X. Qiu, B. Gao, Y. Liu, P. Zhao, and Z. Wang: Biocybern. Biomed. Eng. **41** (2021) 1197. <https://doi.org/10.1016/j.bbe.2021.08.008>
- 7 Y. L. Hsieh, X. Wang, X. Xu, Y. Wu, S. Wang, D. Yu, Y. C. Hsieh, and W. Wang: Sens. Mater. **33** (2021) 3439. <https://doi.org/10.18494/SAM.2021.3519>
- 8 S. Tian, L. Wang, J. Yang, R. Mao, Z. Liu, and Y. Fan: J. Biomech. **52** (2017) 68. <https://doi.org/10.1016/j.jbiomech.2016.12.012>
- 9 Y. L. Hsieh, X. Xu, Y. Wu, and W. Wang: Laryngoscope Investig. Otolaryngol. **6** (2021) 1436. <https://doi.org/10.1002/lio2.699>
- 10 Y. L. Hsieh, Y. Wu, H. Wang, X. Xu, P. Guo, X. Wang, Y. D. Hsieh, H. Lu, and W. Wang: ORL **84** (2022) 219. <https://doi.org/10.1159/000517610>
- 11 J. Pellerito and J. F. Polak: Introduction to Vascular Ultrasonography (Elsevier, Amsterdam, 2019) 7th ed., Chaps. 1–3.
- 12 A. A. Oqlat, M. Z. Matjafri, N. Suardi, M. A. Oqlat, M. A. Abdelrahman, and A. A. Oqlat: J. Med. Ultrasound **26** (2018) 3. [https://doi.org/10.4103/jmu.jmu\\_11\\_17](https://doi.org/10.4103/jmu.jmu_11_17)
- 13 X. Gao, Y.-L. Hsieh, X. Wang, and W. Wang: Front. Hum. Neurosci. **16** (2022) 862420. <https://doi.org/10.3389/fnhum.2022.862420>
- 14 S. B. Davis and P. Mermelstein: IEEE Trans. Acoust. Speech Signal Process. **28** (1980) 357. <https://doi.org/10.1109/TASSP.1980.1163420>
- 15 Y. L. Hsieh, X. Gao, X. Wang, F. C. Hsiang, X. Sun, and W. Wang: Front. Bioeng. Biotechnol. **9** (2022) 777648. <https://doi.org/10.3389/fbioe.2021.777648>
- 16 X. Qiu, P. Zhao, Z. Mu, C. Dai, X. Li, N. Xu, H. Ding, S. Gong, Z. Yang, B. Gao, and Z. Wang: Front. Hum. Neurosci. **16** (2022) 823455. <https://doi.org/10.3389/fnhum.2022.823455>
- 17 H. Ding, P. Zhao, H. Lv, X. Li, X. Qiu, R. Zeng, G. Wang, Z. Yang, S. Gong, L. Jin, and Z. Wang: Neurosurgery **89** (2021) 549. <https://doi.org/10.1093/neuros/nyab222>
- 18 S. Y. Lee, M. K. Kim, Y. J. Bae, G. S. An, K. Lee, B. Y. Choi, J. W. Koo, and J. J. Song: Sci. Rep. **10** (2020) 18194. <https://doi.org/10.1038/s41598-020-75348-3>
- 19 S. C. Joseph, E. Rizk, and R. S. Tubbs: Anatomy, Imaging and Surgery of the Intracranial Dural Venous Sinuses, R. S. Tubbs, Ed. (Elsevier, New York, 2020) pp. 205–220. <https://doi.org/10.1016/B978-0-323-65377-0.00025-8>

## About the Authors



**Yue-Lin Hsieh** received his M.D. degree in 2019 and completed a three-year residency training program at the Fudan University-affiliated Eye & ENT Hospital, Department of Otorhinolaryngology–Head and Neck Surgery from 2016 to 2019. He is currently a Ph.D. student of Fudan University. He is particularly dedicated to clinical management and biomedical investigation of pulsatile tinnitus. Cerebrospinal fluid/dural venous sinus hemodynamics, endolymphatic hydrops, and middle ear mechanics are also his research interests. ([tb22521208@hotmail.com](mailto:tb22521208@hotmail.com))



**Yue-Da Hsieh** received his M.D. degree in 2021 from London School of Economics and Political Science, Department of Economics. He currently works as a macroeconomic scenario risk analyst in Citibank, United Kingdom. He specializes in mathematical economics, statistics, and econometrics, including game theory, contract theory, and time series analysis. He devotes his time to researching time series analysis and mathematical modeling.



**Wuqing Wang** received his Ph.D. degree from the Fudan University-affiliated Eye & ENT Hospital, Department of Otorhinolaryngology–Head and Neck Surgery, China, in 2003. He has been a professor of otolaryngology–head and neck surgery and chief of endoscopic ear surgery in the Division of Neurotology and Skull Base Surgery of the Fudan University-affiliated Eye & ENT Hospital since 2020. He is currently a leading otologic surgeon specializing in endoscopic ear surgery in China. He is a member of the International Working Group on Endoscopic Ear Surgery (IWGEES), Association for Research in Otolaryngology, American Academy of Otolaryngology–Head and Neck Surgery, The International Association of Physicians in Audiology, and the Bárány Society. His current research interests involve surgical management and biomedical investigation of chronic otitis media, Ménière’s disease, vestibular migraine, endolymphatic hydrops, idiopathic sudden sensorineural hearing loss, and pulsatile tinnitus. ([wwuqing@189.cn](mailto:wwuqing@189.cn), [wwuqing@eent.shmu.edu.cn](mailto:wwuqing@eent.shmu.edu.cn))